


Multimodal neuroimaging of gliomatosis cerebri: a case series of four patients

Acta Radiologica Open
9(8) 1–11
© The Foundation Acta
Radiologica 2020
Article reuse guidelines:
sagepub.com/journals-permissions
DOI: 10.1177/2058460120942789
journals.sagepub.com/home/arr



Robin Bonomi¹ , Flora John², Suketu Patel³,
Geoffery Barger^{1,3}, Natasha Robinette^{1,3}, Alit J Amit-Yousif^{1,3},
Michael Dominello^{1,3} and Csaba Juhasz^{1,2,3}

Abstract

In the latest World Health Organization classification of brain tumors, gliomatosis cerebri has been redefined to varying subsets of diffuse gliomas; however, the term is still used to describe gliomas with infiltrative growth into three or more cerebral lobes. These tumors are frequently misdiagnosed and difficult to treat due to their atypical presentation using structural imaging modalities including computed tomography and T1/T2-weighted magnetic resonance imaging (MRI). In this retrospective case series, we compared clinical MRI to amino acid positron emission tomography (PET) to assess the potential value of PET in the assessment of the extent of tumor involvement and in monitoring disease progression. We report the clinical course and serial multimodal imaging findings of four patients. Each patient presented at varying points in disease progression with widespread glioma brain involvement and was evaluated at least once by amino acid PET using alpha-¹¹C-methyl-L-tryptophan (¹¹C-AMT). Increased uptake of ¹¹C-AMT was detected in a subset of non-enhancing brain lesions and detected tumor invasion before MRI signs of tumor in some regions. Increased uptake of ¹¹C-AMT was also detected in tumorous regions not detected by perfusion MRI or MR spectroscopy. Metabolic response to treatment was also observed in two patients. Overall, these data are consistent with and expand upon previous reports using other amino acid PET tracers in gliomatosis and show the potential added value of this imaging modality to clinical MRI in the detection and monitoring of these diffusely infiltrative tumors.

Keywords

Positron emission tomography, magnetic resonance imaging, neuroimaging, amino acid, [¹¹C]-AMT, gliomatosis, glioma

Received 17 May 2020; accepted 23 June 2020

Introduction

Gliomas typically present as a focal mass in one area of the brain; however, they may also be diffuse in nature, either at presentation or upon progression. In rare cases, the glioma is diffusely infiltrative throughout multiple cerebral lobes and without a circumscribed mass (1). Gliomatosis cerebri has been defined as gliomas with widespread growth involving three or more cerebral lobes and frequent extension into infratentorial structures (1). Gliomatosis cerebri has been removed from the most recent 2016 World Health Organization (WHO) classification and is now placed into several diffuse glioma subtypes (2); however, the term is still used widely today. Infiltration throughout the white matter represents the progression of an initial lesion in many cases, but gliomatosis can also present with multifocal tumors (3,4).

Gliomatosis histologically fits within grades II–IV, and the prognosis is worse than that of a localized glioma with the same histologic grade (5). The median progression-free and overall survival for these types of tumors are 10 and 13 months, respectively, with a five-year survival of 18% (5). Due to the

¹Departments of Pediatrics, Neurology, Radiology, Oncology, Wayne State University, Detroit, MI, USA

²PET Center and Translational Imaging Laboratory, Children's Hospital of Michigan, Detroit, MI, USA

³Karmanos Cancer Institute, Detroit, MI, USA

Corresponding author:

Csaba Juhasz, PET Center and Translational Imaging Laboratory, Children's Hospital of Michigan, 3901 Beaubien Street, Detroit, MI 48201, USA.

Email: csaba.juhasz@wayne.edu



widespread disease within the brain, complete surgical removal of these tumors is extremely difficult or impossible. Therefore, treatment regimens rely heavily on combination chemotherapy and radiotherapy (CRT), with the standard therapy consisting of radiotherapy (RT) with concomitant temozolomide (TMZ) (3). In many cases, RT is given as whole brain radiation due to the lack of focal mass or resection cavity. Some studies have demonstrated improved survival in patients receiving a RT dose of 60 Gy. In contrast, survival benefit was not seen with chemotherapy alone (3).

Due to the difficulty in identifying and treating gliomatosis, multiple imaging modalities are often used to obtain accurate diagnosis, optimize treatment regimens, and monitor disease progression. Developments with magnetic resonance imaging (MRI), including spectroscopy (MRS), fluid-attenuated inversion recovery (FLAIR) sequences, and diffusion-weighted imaging (DWI) have led to improved detection of non-contrast enhancing infiltrative gliomas. Additional imaging includes positron emission tomography (PET) with ^{18}F -fluorodeoxyglucose (FDG-PET) (6) and amino acid-based PET ligands that target amino acid transport and, in some cases, alternative cellular energy pathways. Amino acid PET can detect glioma infiltration and assist prognostication in non-enhancing gliomas (7), but there have been only limited studies to define the role of amino acid PET in patients with gliomatosis (8–14).

In our center, the amino acid radiotracer alpha- ^{11}C methyl-L-tryptophan (^{11}C -AMT) has been successfully used to identify and monitor epileptic and tumorous lesions in the brain (15–23). Tryptophan is an essential amino acid for protein synthesis; however, within the brain most of the tryptophan enters alternative pathways to produce serotonin, melatonin, tryptamine, and kynurenine (KYN). The KYN pathway is generally regarded as a pro-inflammatory pathway and its activity is increased with glioma progression (24). Within this pathway, indoleamine 2,3-dioxygenase 1 (IDO1), indoleamine 2,3-dioxygenase 2 (IDO2), and tryptophan 2,3-dioxygenase 2 (TDO2) form the rate limiting step of tryptophan conversion to KYN. IDO1 and TDO2 activity can lead to an immunosuppressed tumor microenvironment that promotes progression of glioblastoma (24). Production of KYN increases the occupancy of the aryl hydrocarbon receptor, thus enhancing the invasiveness of human glioblastoma cells (24,25).

Here, we present the data of four patients with extensive multi-lobar glioma infiltration of varying histologic grades, who have all undergone multiple imaging studies including 1–3 rounds of ^{11}C -AMT-PET. These data are compared with clinical MRI findings

as well as clinical course to illustrate the potential added value of ^{11}C -AMT-PET. We also briefly review the limited literature reporting on the use of other amino acid tracers in imaging gliomatosis cerebri.

Case studies

Patient 1

Initial clinical presentation and MRI: A 29-year-old Indian woman presented with a seizure, prompting an MRI scan which revealed diffuse hyperintensities across both frontal lobes and a small area of increased contrast enhancement in the posterior right frontal lobe. MRS demonstrated elevated choline and reduced N-acetylaspartate (NAA) in the left temporal lobe and right frontal lobe, indicative of neoplastic processes. An excisional biopsy of the right frontal lesion revealed WHO grade II diffuse astrocytoma. Due to the diffuse nature of her disease, complete surgical resection was not a viable option, so she was followed with serial MRI until progression, at which time TMZ was started.

Clinical course and follow-up imaging: Over the next 3.5 years (2003–2007), the patient was followed by serial scans and received 10 cycles of TMZ until clinical progression. MRI at this time demonstrated an increase in size of the right frontal lobe contrast-enhancing lesion (from 3.3×2.3 cm to 5.1×3.1 cm in a seven-month period in 2007) with concordant increases in glucose metabolism on FDG-PET. After resection of the symptomatic FDG-avid mass, pathology classification changed to a WHO grade III anaplastic oligoastrocytoma.

Clinical progression was noted again three years later, with MRI demonstrating several new areas of contrast enhancement in the left insula, indicative of new lesions, which were treated with GammaKnife to 18 Gy. However, within six months, this lesion increased in size, contrast enhancement, and relative cerebral blood volume (rCBV) on perfusion MRI. The patient was treated with tomotherapy (intensity modulated RT) to 50 Gy in 25 fractions which succeeded in decreasing the left insular lesion size.

^{11}C -AMT-PET abnormalities extended beyond MRI-positive lesions: In 2011, an ^{11}C -AMT-PET was done under a research protocol approved by the Human Investigation Committee of Wayne State University. The PET scan demonstrated increased uptake in the right frontal and parietal lobes (standardized uptake value [SUV] tumor/normal cortex ratios = 1.36 and 1.21, respectively) and left temporal lobe and insula (SUV ratios = 1.23 and 1.24, respectively) (Table 1, Fig. 1). MRI of the right frontal lobe also demonstrated increased T2/FLAIR signal and

Table 1. Clinical data, tumor characteristics, and imaging (MRI, PET) findings of the four patients (lesions with increased SUV on PET are listed).

Patient	Gender	Age (years)	Tumor type	Grade	Glioma markers	Survival (days after first PET)	MRI date	MRI findings	AMT-PET date	AMT-PET findings (SUV ratio)
1	F	37	Mixed, oligo-predominant	III	N/A	681	3 April 2011	Cystic lesion with enhancement in L insula and increased nodular intensity in posterior/inferior L insula. FLAIR hyperintense areas in lateral R frontal, R parietal, L temporal and paramedian R parietal	19 May 2011	R parietal (1.36), medial L frontal (1.21), L insula (1.24), inferior L temporal (1.23)
							30 July 2011	L insula cystic lesion is stable. FLAIR/T2 alterations in L frontal with increased rCBV and abnormal MRS		
							20 November 2011	Stable L insular cystic lesion, increase enhancement in L frontal, L insula, medial L temporal		
							27 December 2011	FLAIR/T2-hyperintensities and peripheral enhancing lesion in L frontal. Increased enhancement and rCBV in the L corona radiata and subependyma of L lateral ventricle	19 January 2012	R parietal (1.37), medial L frontal (1.13), L insula (1.31), inf L temporal (1.15)
							21 July 2012	Increased enhancement in L temporal and insula. Stable cystic lesion and enhancing lesion in L frontal and R frontal, stable non-enhancing lesions in R parietal		
							9 October 2012	Worsening enhancement in L temporal, thalamus, and insula with restricted diffusion, abnormal MRS. New nodular enhancing lesion in R frontal resection bed		
2	F	70	Astro/GBM	III-IV	IDH1/2 wild-type; MGMT-meth. 15%	245	3 November 2017	Enhancement with increased rCBV and abnormal MRS in L thalamus and L temporal lobe and peritrigonal WM. Non-enhancing lesion in R thalamus, without rCBV or MRS changes	8 November 2017	L thalamus (3.96), R thalamus (1.4)
							19 January 2018	No change in L and R thalamus lesions. Scattered FLAIR/T2 hyperintense areas in L insula and external capsule		

(continued)

Table 1. Continued.

Patient	Gender	Age (years)	Tumor type	Grade	Glioma markers	Survival (days after first PET)	MRI date	MRI findings	AMT-PET date	AMT-PET findings (SUV ratio)
3	M	24	Oligo	II	No 1p/19q co-deletion, IDH1/2 wild-type, No MGMT-meth.	197	30 June 2017	Large irregular enhancement in L temporal with decreased rCBV and MRS abnormalities. Persistent diffuse confluent FLAIR hyperintensity in supratentorial WM (L>R), corpus callosum and brainstem. R midline shift.	19 July 2017	L temporal (1.74)
							12 March 2018	Stable R and L thalamus lesions. New enhancing punctate focus in L temporal. 6-mm right midline shift.		
							31 August 2017	Slight decrease of enhancement in L temporal lobe	21 September 2017	L temporal (1.38)
							14 November 2017	Stable enhancement of L temporal, thickened splenium of corpus callosum with subtle enhancement		
							24 January 2018	Stable enhancement of L temporal, new enhancing lesion in L frontal underlying the motor cortex (ischemia > glioma)		
4	M	61	GBM	IV	IDH1 wild-type no MGMT-meth.	240	14 February 2017	Increased enhancing nodules in L thalamus with confluent FLAIR/T2 signal alteration in the L frontal, temporal and parietal. Small stable DVM in R frontal	13 February 2017	L temporal (2.5), R frontal (DVM) (1.6)
							24 April 2017	Decreased enhancement surrounding L temporal, MRS abnormality in adjacent white matter.	25 April 2017	R frontal (1.6), L temporal (1.4)
							22 May 2017	Subtle increase in size of FLAIR/T2 hyperintense mass in R frontal with patchy enhancement and increased rCBV. Increased nodular enhancement in L temporal		
							25 July 2017	R frontal lesion increased in size, tumor in anterior inferior R frontal, multiple additional lesions in R frontal	27 July 2017	R frontal (2.49), L temporal (1.78), L frontal (1.98), R frontal periventricular (1.86), R frontal (1.97) high R frontal (2.2)

MRI, magnetic resonance imaging; MRS, magnetic resonance spectroscopy; N/A, not applicable; PET, positron emission tomography; rCBV, relative cerebral blood volume; SUV, standard uptake value.

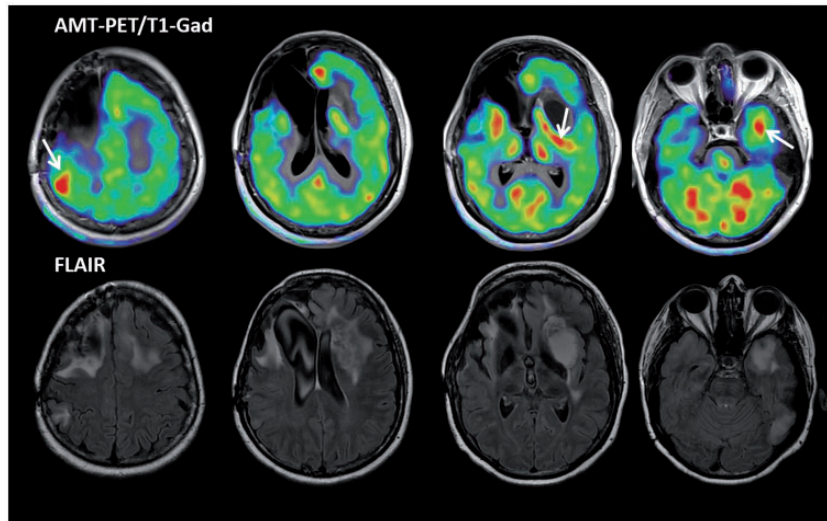


Fig. 1. Representative axial image planes from the 2011 scans of patient 1: co-registered [^{11}C]-AMT-PET/MRI post-gadolinium (T1-gad) images in the upper panel and corresponding FLAIR images in the lower panel. The images demonstrate multiple [^{11}C]-AMT-accumulating lesions in the right parietal, left medial frontal, left insular, and left inferior temporal regions (arrows), which also showed an increased signal on FLAIR images but no contrast enhancement. FLAIR showed additional brain regions with high signal but low uptake of [^{11}C]-AMT, consistent with edema. Note that high uptake of [^{11}C]-AMT in the basal ganglia, occipital cortex, and cerebellum is physiologic.

continued worsening in the left temporal lobe and insula with increased rCBV and elevated choline/creatinine ratios on MRS. Notably, the AMT-positive right parietal lesion was not picked up on MR studies.

In 2012, MRI demonstrated continued worsening of the left temporal and insular lesions with FLAIR signal alteration now spreading into the thalamus and peritrigonal white matter. A repeat [^{11}C]-AMT PET scan was consistent with these findings and highlighted increased activity within the right parietal region. The patient died in late 2012, almost 10 years after her initial disease presentation.

Patient 2

Initial clinical presentation, MRI, and [^{11}C]-AMT-PET: A 69-year-old Caucasian woman presented to an outside Emergency Department (ED) with confusion and fever and was found to be septic with pneumonia and treated with antibiotics. At the time of transfer to our institution, the patient was intact neurologically, but MRI demonstrated multiple contrast enhancing lesions in the left hemisphere (thalamus, temporal lobe, and peri-trigonal white matter). The largest of these was a heterogeneous 4.4 cm mass in the left thalamus. Increased rCBV and MRS abnormalities were consistent with a high-grade glial neoplasm. Additionally, a right thalamic mass of 3.2 cm, which was non-enhancing and without rCBV or MRS abnormalities, was also visualized. [^{11}C]-AMT-PET

demonstrated severely increased radiotracer uptake in the left posterior thalamus (SUV ratio = 3.96), with additional uptake extending into the adjacent white matter. A separate area with a moderately increased uptake (SUV ratio = 1.4) was found in the non-enhancing right thalamic lesion (Table 1, Fig. 2).

Biopsy of the smaller left temporal lesion confirmed WHO grade III anaplastic astrocytic diffusely infiltrative glioma. Molecular analysis demonstrated wild-type isocitrate dehydrogenase 1 and 2 (IDH1 and 2), and O⁶-methylguanine-DNA-methyltransferase (MGMT) promoter methylation of 15%.

Clinical course and follow-up MRI: The patient could not complete the prescribed full courses of CRT due to the development of bilateral pulmonary emboli. Within the next six weeks, the patient received partial brain radiotherapy to 60 Gy and TMZ doses off and on at the reduced dosage of 140 mg/day for a total of three weeks.

Seven months after the initial diagnosis, MRI demonstrated new nodular enhancement in the left posterolateral thalamus and left external capsule but remained inconclusive whether this was due to radiation injury or infiltrating tumor. The final MRI one month later, after clinical worsening, demonstrated extensive FLAIR hyperintensities throughout both hemispheres and a 6-mm rightward midline shift, although the two thalamic lesions remained stable. She died shortly thereafter at 18 months after the original diagnosis.

Patient 3

Initial clinical presentation and MRI: A 24-year-old African American man presented to the ED with changes in speech, loss of appetite, memory difficulty, occasional nausea, and vomiting over three months. Physical examination revealed right-sided upper and lower extremity weakness, significant gait imbalance, and papilledema. MRI demonstrated a right midline shift with widespread enhancing lesions involving bilateral frontal, parietal, and temporal lobes, as well as left occipital lobe, while MRS was notable for elevated choline and diminished NAA peaks within the left temporal region. Biopsy of the left temporal lobe mass

demonstrated a tumor that was histologically consistent with a WHO grade II oligodendroglioma, although negative for IDH1/2 mutation, no MGMT promoter methylation, and no 1p/19q co-deletion.

Clinical course and follow-up MRI: Shortly after the biopsy, he developed complete right hemiparesis and began intensive rehabilitation. Whole brain RT (45 Gy in 25 fractions) was initiated followed by tomotherapy boost (900 cGy in five fractions) to the left temporal region for a total dose of 54 Gy. Symptoms stabilized following treatment and the patient began carboplatin (five days of treatment dose every 28 days) therapy.

Five months after the biopsy an MRI demonstrated an irregular, heterogeneously enhancing $5.4 \times 3.7 \times 3.5$ cm left temporal lobe mass with worsening FLAIR and T2 signal alteration and continued 4-mm rightward midline shift with additional left uncus herniation. Left temporal lobe MRS demonstrated increased choline, reversal of Hunter's angle, and abnormal lipid lactate levels, all suggesting high-grade glial tumor. However, perfusion imaging showed decreased rCBV within the left temporal lobe/insula region, which was more consistent with radiation injury rather than high-grade glioma.

[¹¹C]-AMT-PET supported tumor progression and detected treatment response: [¹¹C]-AMT-PET demonstrated a small, focal hotspot with increased radiotracer accumulation posterior to the radiated left temporal tumor (SUV ratio = 1.74) (Table 1, Fig. 3). This PET finding supported tumor progression rather than radiation injury. Bevacizumab treatment was added to his carboplatin, and follow-up MRIs two and four months later showed stable lesions. Repeat [¹¹C]-AMT-PET two months after the initial PET scan also showed decreased radiotracer uptake in the left temporal lesion (SUV ratio = 1.38).

The temporal lobe mass and the associated white matter signal alterations remained stable on subsequent MRIs; however, a new lesion developed in the

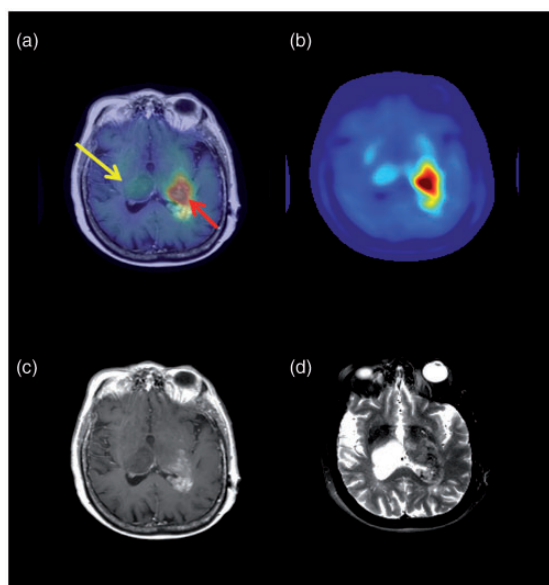


Fig. 2. Representative axial brain images for patient 2. (a) T1 MRI with gadolinium fused with [¹¹C]-AMT-PET image, the red arrow highlights the left contrast-enhancing thalamic lesion with SUV ratio of 3.96, the yellow arrow highlights the right non-enhancing thalamus lesion with an SUV ratio of 1.4. (b) [¹¹C]-AMT-PET image (c) T1 gadolinium image, (d) T2 image.

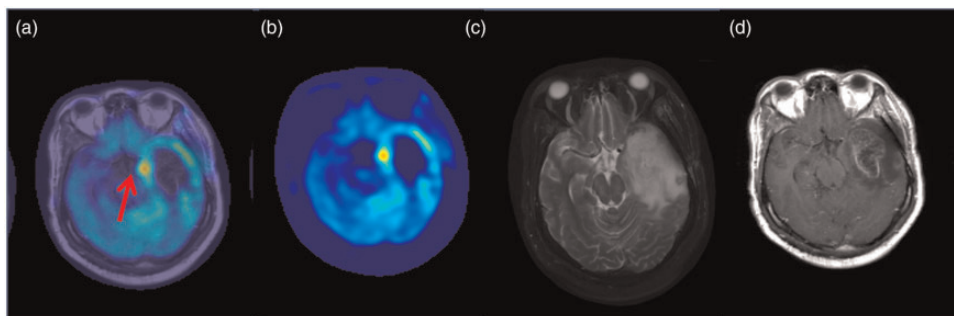


Fig. 3. Representative axial images for patient 3 from July 2017. (a) T1 MRI with gadolinium fused with [¹¹C]-AMT-PET image, with the red arrow highlighting the left medial temporal lesion with SUV ratio of 1.74. (b) [¹¹C]-AMT-PET image, (c) T2/FLAIR image, (d) T1 post-gadolinium image.

subcortical white matter underlying the motor cortex. He continued to clinically decompensate with worsening motor and verbal skills over the next few months and died 20 months after disease presentation.

Patient 4

Initial clinical presentation and MRI: A 60-year-old Caucasian man presented to an outside hospital with chest pain, left arm pain, and difficulty speaking. MRI demonstrated a heterogeneously enhancing 4.2-cm left temporal lobe mass with surrounding vasogenic edema and moderate mass effect. Upon admission to our institution, he presented with dense receptive aphasia and difficulty word finding without sensory-motor deficits. The patient underwent volumetric resection of the left temporal mass, and histopathology confirmed WHO grade IV astrocytic glioma (glioblastoma) with wild-type IDH1/2 and no MGMT promoter methylation.

Clinical course and follow-up MRIs: One month later, MRI demonstrated nodular enhancement within the posterior medial wall of the resection cavity and T2/FLAIR signal alteration in the left frontal lobe. He began treatments of TMZ (140 mg/day) and RT (planned 60 Gy/30 fractions). Unfortunately, he was admitted to the hospital for bilateral foot

abscesses and all treatments were held after 10 Gy of RT and one dose of TMZ.

Four months later, a repeat MRI demonstrated that the nodular enhancement along the posterior resection cavity wall had decreased and the left frontal lobe remained stable. His original treatments were resumed, and the patient completed the planned CRT. On follow-up imaging, FLAIR and T2 signal intensity changes were seen in the left temporal lobe resection bed concerning for tumor progression.

Serial [^{11}C]-AMT-PET supported tumor progression, detected treatment response followed by development of new tumor foci: [^{11}C]-AMT-PET demonstrated increased uptake in the left temporal region (SUV ratio = 2.5) (Table 1, Fig. 4). Additionally, increased uptake (SUV ratio = 1.6) was noted in the right inferior frontal cortex, which corresponded to a developmental venous malformation (DVM) seen on MRI.

About four months later, the patient began tumor treating fields (TTFields) therapy, delivered by the Optune[®] device, along with a bi-weekly course of bevacizumab and irinotecan. After 90 days of these interventions, follow-up MRI and [^{11}C]-AMT-PET demonstrated improvement in the left temporal lobe lesion (SUV ratio = 1.4). However, a new focus with

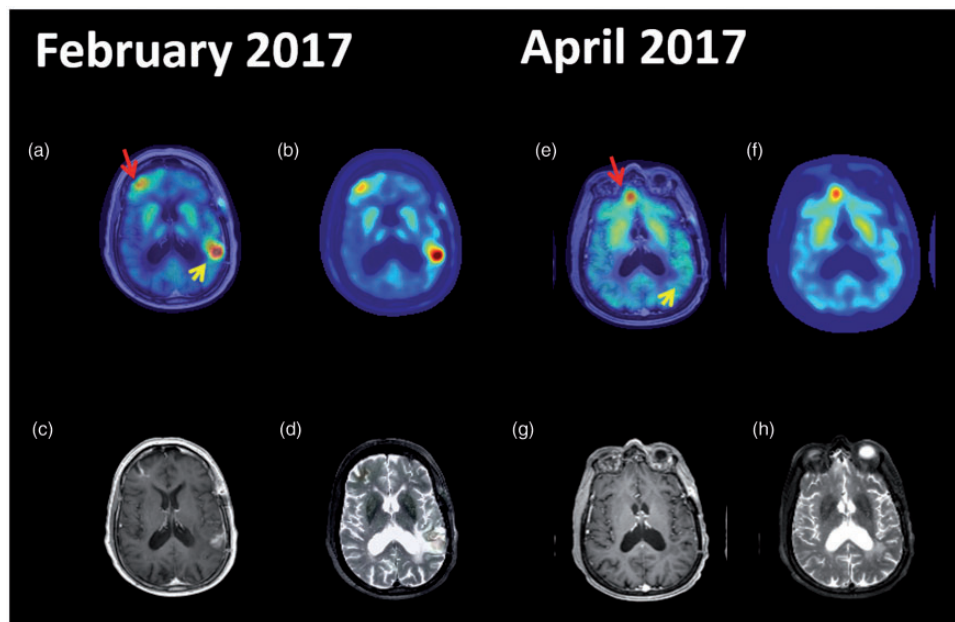


Fig. 4. Representative axial images for patient 4 from February 2017, before receiving TTFields therapy (a–d) and from April 2017, two months after starting TTFields treatment combined with bevacizumab and irinotecan (e–h). (a) T1 post-gadolinium MRI fused with [^{11}C]-AMT-PET image, the yellow arrow highlights the left temporal lesion with SUV ratio of 2.5 and the red arrow highlighting the right frontal DVM lesion (SUV ratio of 1.6). (b) [^{11}C]-AMT-PET image, (c) T1 gadolinium image, (d) T2 image. Repeated AMT-PET in April 2017 showed a new area with high uptake of [^{11}C]-AMT in the right inferior medial region (SUV ratio = 1.6). (e) T1 MRI with gadolinium fused with [^{11}C]-AMT-PET image, red arrow highlighting the new frontal lesion. The left temporal lesion showed a decreased SUV ratio (1.4) compared to the first study. (f) [^{11}C]-AMT-PET image, (g) T1 gadolinium image, (h) T2 image. TTFields, Tumor Treatment Fields.

increased uptake of [^{11}C]-AMT was detected in the right medial inferior frontal lobe (SUV ratio = 1.6) (Table 1, Fig. 5), which was not seen on MRI at this time. MRS detected abnormal metabolism in left peritrigonal white matter adjacent to the temporal lobe tumor resection bed, consistent with high-grade glial neoplasm.

One year after his initial diagnosis, the patient had increased frequency and severity of headaches, vision loss, difficulty of speech, and decreased hearing. TTFIELDS compliance became suboptimal (<18 h/day) and the irinotecan was stopped, while bevacizumab was continued. An MRI scan revealed increased size of the lesions in the right frontal lobe and spread to the left frontal lobe. The corresponding, third [^{11}C]-AMT-PET scan showed worsening in the original temporal lobe lesion, as well as three new foci in the right frontal lobe (SUV ratios >1.85 in all) and one in the left frontal lobe (SUV ratio = 1.98) (Table 1, Fig. 5). He continued to decline and died one month later.

Discussion

The serial imaging findings of the presented four patients demonstrate the potential utility of amino acid PET in both the early and late clinical course of gliomatosis. These findings are largely consistent with previous reports using PET imaging with a variety of

other amino acid tracers in patients with gliomatosis (Table 2). [^{11}C]-methionine ([^{11}C]-MET) PET study demonstrated high tracer uptake to extend beyond the CT- and MRI-detected tumor and showed good correspondence between dense tumor infiltration on histopathology and high [^{11}C]-MET uptake on PET (11). A subsequent [^{11}C]-MET PET study also demonstrated increased radiotracer accumulation in type II gliomatosis (with an obvious mass) but low uptake in a type I lesion (without a well-defined mass) (12). Monitoring disease progression using [^{11}C]-MET after radiotherapy has also been successful (10), as amino acid PET may be more sensitive to tumor progression than MRI. For example, 3-[F-18]- α -methyl-tyrosine PET detected a glioma two years before a visible MRI lesion (13) and increased accumulation of [^{11}C]-MET and [^{11}C]-choline within the tumor lesions demonstrated improved detection of tumor margins compared to other imaging modalities (14). A more recent study of pediatric astrocytic gliomas included five cases of gliomatosis cerebri, where ^{18}F -3,4-dihydroxyphenylalanine [^{18}F]-DOPA showed increased uptake in the tumor regions (26) and affected management by differentiating tumor from treatment-related changes or by guiding targeted biopsy. Altogether, these studies support the clinical use of amino acid PET, regardless of the radiotracer used.

Prior studies from our institution have indicated the clinical utility of [^{11}C]-AMT-PET imaging for

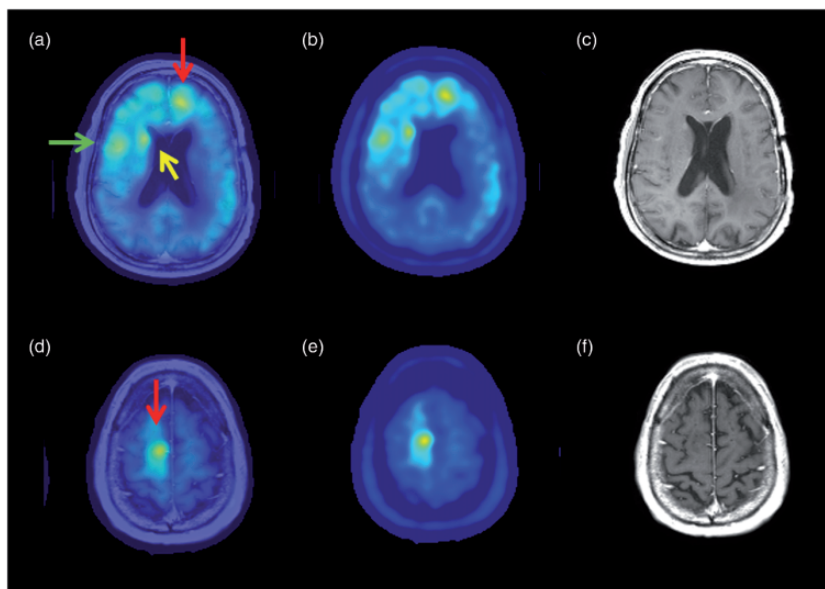


Fig. 5. Representative images for patient 4 from July 2017 demonstrating additional, non-enhancing lesions with increased uptake of [^{11}C]-AMT including left frontal (red arrow, SUV ratio = 1.98), right periventricular (yellow arrow, SUV ratio = 1.86), and right frontal (green arrow, SUV ratio = 2.49) lesions that emerged during continuing TTFIELDS therapy: (a) T1 MRI with gadolinium fused with [^{11}C]-AMT-PET image with three new frontal lesions highlighted. (b) [^{11}C]-AMT-PET image, (c) T1 gadolinium image. (d) T1 MRI with gadolinium fused with [^{11}C]-AMT-PET image of a new high right frontal lesion highlighted by red arrow (SUV ratio = 2.2); (e) [^{11}C]-AMT-PET image, (f) T1 MRI with gadolinium image.

Table 2. Summary of the main findings of studies reporting on amino acid PET findings in patients with gliomatosis.

Author	Journal (year)	Patients (n)	Age (years)	Amino acid PET tracer used	Main findings
Mineura et al.	J Nucl Med (1991)	1	32	[C-11]-methionine	High uptake extending beyond CT and MRI lesions Histopathology verified dense tumor infiltration in PET+ regions
Plowman et al.	Br J Neurosurg (1998)	2	12–38	[C-11]-methionine	Low uptake in both cases
Shintani et al.	J Neurol Sci (2000)	1	19	[C-11]-methionine	High uptake in MRI-detected lesions Interval decrease of uptake after radiotherapy
Sato et al.	Neuroradiology (2003)	8	15–60	3-[F-18]- α -methyl-tyrosine	High uptake with 7 patients with gliomatosis; higher than FDG uptake Low uptake in 1 patient (had severe intracranial hypertension) Tumor detection two years before MRI lesion in one patient
Desclée et al.	J Neuroradiol (2010)	3	12–73	[C-11]-methionine	High uptake in two type II; low uptake in one type I
Pichler et al.	EJNMMI (2010)	2*	22–?	O-(2-[F-18]-fluoroethyl)-L-tyrosine	Low uptake in both cases (WHO grade III)
Cai et al.	Clin Nucl Med (2011)	1	12	[C-11]-methionine	High uptake in portions of T2-positive, low FDG-uptake region
Morana et al.	J Nucl Med (2014)	5*	6–17	[F-18]-DOPA	Markedly (n = 4) or moderately (n = 1) increased uptake Affected management in n = 3 (guided biopsy side (n = 1) or differentiated tumor from treatment-related changes (n = 2)).

*Gliomatosis cases in a larger glioma series.

differentiating glioblastoma progression from radiation injury (19) and detection of tumor infiltration (22). In the former study, a SUV ratio of 1.65 was used to define recurrent high-grade glioma from radiation injury. Furthermore, tumor/cortex SUV ratio of 1.36 was used to differentiate gliomas from non-glioma tissue (edema) in pretreatment cases (27). This is especially relevant for patient 1, where areas of unknown significance on MRI corresponded with [¹¹C]-AMT-PET increased uptake. For example, new modest uptake (SUV ratio = 1.31) was visible in the left insular cortex but using MRI this area remained stable without interval. However, six months later, MRI progression was evident with increased lesion enhancement and FLAIR abnormalities. In the left medial frontal cortex [¹¹C]-AMT-PET demonstrated a mild increase (SUV ratio = 1.21) before MRI scans finding new

nodular enhancement in this region, suggesting that even mild [¹¹C]-AMT increases may represent infiltrating glioma in such patients. Furthermore, ratios below 1.4 may predict slow progression and prolonged survival.

Imaging with [¹¹C]-AMT-PET in patient 2 detected gliomatosis in a non-contrast enhancing lesion when rCBV and MRS did not indicate active tumor. Subsequent MRI demonstrated tumor progression with bilateral FLAIR hyperintensities and a 6-mm right midline shift, suggestive of widespread tumor infiltration.

In patients 3 and 4, serial [¹¹C]-AMT-PET detected an initial response to treatment a change in therapy (bevacizumab in patient 3 and Optune combined with bevacizumab and irinotecan in patient 4). Patient 4 used TTFields for three months with adjuvant

chemotherapy (bevacizumab and irinotecan). This combination led to a marked reduction in [^{11}C]-AMT accumulation within the temporal lobe lesion, but high uptake of [^{11}C]-AMT emerged in the right frontal lobe, an area not directly under TTFields therapy. In this case, [^{11}C]-AMT imaging before and after treatment allowed monitoring of tumor metabolism with higher sensitivity to tumor growth or regression than MRI alone. Amino acid PET has previously monitored treatment efficacy during bevacizumab and TTFields therapy in glioblastomas (20,28). TTFields has also been successful at reducing tumor burden and symptoms in glioblastoma (29). Taken together, these cases demonstrated that amino acid PET with [^{11}C]-AMT can provide increased sensitivity for tumor progression and monitor response to gliomatosis treatment.

Increased tumoral accumulation of [^{11}C]-AMT may be due to increased activity of the large amino acid transporter 1 (LAT1), which is often upregulated early in brain tumor progression to transport tryptophan across the blood–tumor barrier (30). The same transport system drives tumoral accumulation of other commonly used amino acid PET tracers in neuro-oncology (31). Tumoral [^{11}C]-AMT accumulation may also represent an increase in key enzymes of the immunosuppressive kynurenine pathway (32,33). While upregulation of these enzymes (such as IDO1/2 and TDO2) is common in glioblastomas, little is known of the activity of these enzymes in gliomatosis. The data presented here suggest that [^{11}C]-AMT-PET can provide complementary information to conventional MRI and to advanced sequences such as MRS or perfusion imaging. MRS is inherently limited by brain sampling, which is of greater importance in multifocal tumors like gliomatosis. This was illustrated in patients 1 and 2 with multiple [^{11}C]-AMT-positive lesions that were incompletely sampled by MRS. Perfusion MRI can detect high-grade tumors and differentiate malignant glioma progression from radiation injury, but it has limited ability to detect tumor-infiltrated brain, especially with grade II–III gliomas. Patients 1, 2, and 3 had multiple [^{11}C]-AMT-positive lesions with low rCBV, detected by perfusion MRI.

In conclusion, this case series describes the clinical course and imaging findings, including [^{11}C]-AMT-PET in four patients with gliomatosis. While their treatment was not guided by this imaging modality, this retrospective analysis demonstrates that [^{11}C]-AMT-PET can provide complementary information compared to both conventional and advanced MRI. The scans were predictive of progression in some of these patients, and this may provide valuable information for treatment planning in the future. Amino acid PET can also be used to monitor treatment

response in gliomatosis. Furthermore, use of PET imaging with specific radiotracers may help better understand the molecular pathways in gliomatosis and glioblastoma progression and may lead to further targeted therapies and improved outcomes for patients.

Acknowledgements

The authors acknowledge the contributions of Dr. Mark Szlachy and Dr. William Kupsy of the Karmanos Cancer Institute for their contributions to the patient care and manuscript.

Declaration of conflicting interests

The author(s) declared no potential conflicts of interest with respect to the research, authorship, and/or publication of this article.

Funding

The author(s) disclosed receipt of the following financial support for the research, authorship, and/or publication of this article: This study was supported by grants from the National Institutes of Health / National Cancer Institute (CA 123451 and P30 022453).

ORCID iD

Robin Bonomi  <https://orcid.org/0000-0003-4500-944X>

References

1. Louis DN, Ohgaki H, Wiestler OD, et al. The 2007 WHO classification of tumours of the central nervous system. *Acta Neuropathol* 2007;114:97–109.
2. Louis DN, Perry A, Reifenberger G, et al. The 2016 World Health Organization Classification of Tumors of the Central Nervous System: a summary. *Acta Neuropathol* 2016;131:803–820.
3. Chen S, Tanaka S, Giannini C, et al. Gliomatosis cerebri: clinical characteristics, management, and outcomes. *J Neurooncol* 2013;112:267–275.
4. Zhang CP, Li HQ, Zhang WT, et al. Clinical manifestations and imaging characteristics of gliomatosis cerebri with pathological confirmation. *Asian Pac J Cancer Prev* 2014;15:4487–4491.
5. Georgakis MK, Tsivgoulis G, Spinou D, et al. Prognostic factors and survival of gliomatosis cerebri: a systematic review and meta-analysis. *World Neurosurg* 2018;120:e818–e854.
6. Meric K, Killeen RP, Abi-Ghanem AS, et al. The use of ^{18}F -FDG PET ratios in the differential diagnosis of common malignant brain tumors. *Clin Imaging* 2015;39:970–974.
7. Takano K, Kinoshita M, Arita H, et al. Diagnostic and Prognostic Value of ^{11}C -Methionine PET for Nonenhancing Gliomas. *Am J Neuroradiol* 2016;37:44–50.

8. Plowman PN, Saunders CA, Maisey MN. Gliomatosis cerebri: disconnection of the cortical grey matter, demonstrated on PET scan. *Br J Neurosurg* 1998;12:240–244.
9. Pichler R, Dunzinger A, Wurm G, et al. Is there a place for FET PET in the initial evaluation of brain lesions with unknown significance? *Eur J Nucl Med Mol Imaging* 2010;37:1521–1528.
10. Shintani S, Tsuruoka S, Shiigai T. Serial positron emission tomography (PET) in gliomatosis cerebri treated with radiotherapy: A case report. *J Neurol Sci* 2000;173:25–31.
11. Mineura K, Sasajima T, Kowada M, et al. Innovative approach in the diagnosis of gliomatosis cerebri using carbon-11-L-methionine positron emission tomography. *J Nucl Med* 1991;32:726–728.
12. Desclee P, Rommel D, Hernalsteen D, et al. Gliomatosis cerebri, imaging findings of 12 cases. *J Neuroradiol* 2010;37:148–158.
13. Sato N, Inoue T, Tomiyoshi K, et al. Gliomatosis cerebri evaluated by ¹⁸F-alpha-methyl tyrosine positron-emission tomography. *Neuroradiology* 2003;43:700–707.
14. Cai L, Gao S, Li Y, et al. ¹¹C-Methionine or ¹¹C-Choline PET is superior to MRI in the evaluation of gliomatosis cerebri. *Clin Nucl Med* 2011;36:127–129.
15. Chugani HT, Kumar A, Kupsky W, et al. Clinical and histopathological correlates of ¹¹C-alpha-methyl-L-tryptophan (AMT) PET abnormalities in children with intractable epilepsy. *Epilepsia* 2011;52:1692–1698.
16. Juhasz C, Chugani DC, Muzik O, et al. Alpha-methyl-L-tryptophan PET detects epileptogenic cortex in children with intractable epilepsy. *Neurology* 2003;60:960–968.
17. Juhasz C, Mittal S. Molecular imaging of tryptophan metabolism in tumors. In: Mittal S (ed) *Targeting the broadly pathogenic kynurenine pathway*. Chapter 28. Springer International Publishing: Switzerland, 2015, pp. 373–389.
18. Juhasz C, Chugani DC, Muzik O, et al. In vivo uptake and metabolism of alpha-[¹¹C]methyl-L-tryptophan in human brain tumors. *J Cereb Blood Flow Metab* 2006;26:345–357.
19. Alkonyi B, Barger GR, Mittal S, et al. Accurate differentiation of recurrent gliomas from radiation injury by kinetic analysis of alpha-¹¹C-methyl-L-tryptophan PET. *J Nucl Med* 2012;53:1058–1064.
20. Bosnyak E, Barger GR, Michelhaugh SK, et al. Amino acid PET imaging of the early metabolic response during tumor-treating fields (TTFields) therapy in recurrent glioblastoma. *Clin Nucl Med* 2018;43:176–179.
21. Bosnyak E, Kamson DO, Guastella AR, et al. Molecular imaging correlates of tryptophan metabolism via the kynurenine pathway in human meningiomas. *Neuro Oncol* 2015;17:1284–1292.
22. Bosnyak E, Kamson DO, Robinette NL, et al. Tryptophan PET predicts spatial and temporal patterns of post-treatment glioblastoma progression detected by contrast-enhanced MRI. *J Neurooncol* 2016;126:317–325.
23. John F, Bosnyak E, Robinette NL, et al. Multimodal imaging-defined subregions in newly diagnosed glioblastoma: impact on overall survival. *Neuro Oncol* 2019;21:264–273.
24. Adams S, Teo C, McDonald KL, et al. Involvement of tryptophan metabolism in human glioma pathophysiology. *PLoS One* 2014;9:e112945.
25. Guastella AR, Michelhaugh SK, Klinger NV, et al. Investigation of the aryl hydrocarbon receptor and the intrinsic tumoral component of the kynurenine pathway of tryptophan metabolism in primary brain tumors. *J Neurooncol* 2018;139:239–249.
26. Morana G, Piccardo A, Milanaccio C, et al. Value of ¹⁸F-3,4-dihydroxyphenylalanine PET/MR image fusion in pediatric supratentorial infiltrative astrocytomas: a prospective pilot study. *J Nucl Med* 2014;55:718–723.
27. Kamson DO, Juhász C, Buth A, et al. Tryptophan PET in pretreatment delineation of newly-diagnosed gliomas: MRI and histopathologic correlates. *J Neurooncol* 2013;112:121–132.
28. Ono T, Sasajima T, Doi Y, et al. Amino acid PET tracers are reliable markers of treatment responses to single-agent or combination therapies including temozolomide, interferon-β, and/or bevacizumab for glioblastoma. *Nucl Med Biol* 2015;42:598–607.
29. Stupp R, Taillibert S, Kanner AA, et al. Maintenance therapy with Tumor-Treating Fields plus temozolomide vs temozolomide alone for glioblastoma: A randomized clinical trial. *JAMA* 2015;314:2535–2543.
30. Alkonyi B, Mittal S, Zitron I, et al. Increased tryptophan transport in epileptogenic dysembryoplastic neuroepithelial tumors. *J Neurooncol* 2012;107:365–372.
31. Juhasz C, Dwivedi S, Kamson DO, et al. Comparison of amino acid positron emission tomographic radiotracers for molecular imaging of primary and metastatic brain tumors. *Mol Imaging* 2014;13:7290–2014.
32. Chugani DC, Muzik O. Alpha[¹¹C]methyl-L-tryptophan PET maps brain serotonin synthesis and kynurenine pathway metabolism. *J Neurooncol* 2000;20:2–9.
33. Guastella AR, Michelhaugh SK, Klinger NV, et al. Tryptophan PET imaging of the kynurenine pathway in patient-derived xenograft models of glioblastoma. *Mol Imaging* 2016;15:1536012116644881.